

Finite Element Analysis of Rail-End Bolt Hole and Fillet Stress on Bolted Rail Joints

Kaijun Zhu, Yu Qian, J. Riley Edwards, and Bassem O. Andrawes

A rail joint typically is one of the weakest elements of a track superstructure, primarily because of discontinuities in its geometric and mechanical properties and the high-impact loads induced by these discontinuities. The development of continuously welded rail has significantly reduced the number of rail joints, but many bolted joints remain installed in rail transit systems. Because of the unique loading environment of a rail transit system (especially high-frequency, high-repetition loads), defects related to bolted rail joints (e.g., joint bar failures, bolt hole cracks, and cracks in the upper fillet) continue to cause service failures and can pose derailment risks. Recent research in the Rail Transportation and Engineering Center at the University of Illinois at Urbana–Champaign has focused on investigating crack initiation in the bolt hole and fillet areas of bolted rail joints. Stress distribution was investigated at the rail-end bolt hole and upper fillet areas of standard, longer, and thicker joint bars under static loading conditions. Numerical simulations were organized into a comprehensive parametric analysis performed with finite element modeling. Preliminary results indicated that the longer joint bar performed similarly to the standard joint bar but the thicker joint bar reduced rail vertical displacement and rail upper fillet stresses compared with the standard joint bar. However, the thicker joint bar also may generate higher stresses at the rail-end bolt hole. Additionally, joint bar performance was dependent on the rail profile and bolt hole location.

Rail joints connect two adjacent (end to end) rails. Starting in the 1810s, 45° or 60° miter joints were used. Then, as an improvement, scarf joints were developed; the two rail ends were notched and bolted together. Splice joints were invented in the United States around 1830 and led to the development of angled joint bars in the 1850s. Angled joint bar design spread quickly, was adopted worldwide, and became the standard that has endured to the present (1).

BACKGROUND

Early joint bars were designed to match the profile of the rail section perfectly in a conformal manner (Figure 1) (2–4). However, with the development of materials and manufacturing technologies in the early 20th century, bolted joint bars gradually became thinner at the bolt hole area around the neutral axis to save material but this modification did not significantly decrease the moment of inertia and bending strength of the joint bars (1). In contrast, insulated

joints have retained a thick bar design that conform to the geometry of the rail section since the 1870s (5).

During the 1920s, most joint bars were 20 to 48 in. (50.8 to 121.9 cm) long. Four bolts were used for joint bars 20 to 30 in. (50.8 to 76.2 cm) long, six bolts were used for joint bars 36 to 40 in. (91.4 to 101.6 cm) long, and eight bolts were used for joint bars more than 40 in. (101.6 cm) long (6). The joint bars longer than 36 in. (91.4 cm) became less popular over the years and were deemed unnecessary for typical loading conditions. Currently, the most common joint bars are 24 in. (61.0 cm) or 36 in. (91.4 cm) long.

With the development of continuously welded rail, the number of in-service bolted joints has been reduced significantly; rail joint research also has decreased as a result. However, many bolted joints remain in rail transit systems, especially legacy systems. Because of the unique loading environment in rail transit systems—high-frequency, high-repetition (i.e., number of load replications) wheel loads, heavier than previously seen—defects associated with bolted rail joints still present significant challenges.

In May 2013, a Metro-North passenger train derailed and at least 65 persons were injured. The National Transportation Safety Board determined that the probable cause of the derailment was an undetected broken pair of compromise joint bars (7). In July 2013 in Brétigny-sur-Orge, France, a train derailed and collided with a station platform, causing seven fatalities and more than 200 injuries. This derailment also was caused by a rail joint bar failure (8).

To mitigate defects in bolted rail joints, including broken bolts and cracks in the joint bar, bolt holes, and upper fillet of the rail, recent research efforts have focused on understanding stress distribution, crack initiation, and crack propagation in bolted rail joints. Typically, bolt hole cracks initiate at the end bolt hole of the receiving rail in a direction that is approximately 45° to the neutral axis of the rail (9–11). Previous research identified the primary driving force for bolt hole cracks in bolted joints as positive shear stress around the bolt hole (12, 13). This shear stress is proportional to the wheel–rail impact load and can be magnified further by the stress concentration effect of the hole (12, 13). Carolan et al. (14) found that, other than the number of bolts used in the joints, rail deflection and stress distribution were dependent mostly on the support condition, whereas Zhu et al. (15) concluded that the missing bolts condition affects stress distribution in the rail joint. Even though joint easement reduced contact stress when properly adopted, high contact pressure was still found in the area adjacent to the easement (14). Recent research has focused on studying rail joints with “standard” joint bar configurations; however, the performance of rail joints with nonstandard configurations—longer joint bars, thicker joint bars, and different bolt configurations—has not been studied thoroughly for the current loading environment.

Recent research performed by the Rail Transportation and Engineering Center at the University of Illinois at Urbana–Champaign

Rail Transportation and Engineering Center, Department of Civil and Environmental Engineering, University of Illinois at Urbana–Champaign, 205 North Mathews Avenue, Urbana, IL 61801. Corresponding author: Y. Qian, yuqian1@illinois.edu.

Transportation Research Record: Journal of the Transportation Research Board, No. 2607, 2017, pp. 33–42.
<http://dx.doi.org/10.3141/2607-06>

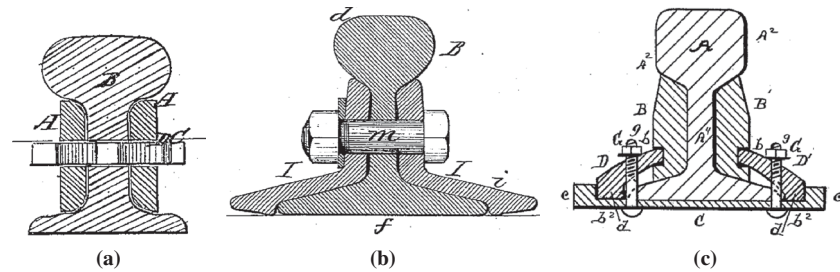


FIGURE 1 Early joint bar designs (2-4).

(UIUC) has focused on investigating the stress distribution around the rail-end bolt hole and upper fillet areas to better understand crack initiation and propagation. Preliminary results are presented in this paper from numerical simulations of bolted joints under a static transit loading condition with four joint bar types.

OBJECTIVE AND SCOPE

This study investigated the stress distribution around the rail joint area, specifically at the bolt hole and upper fillet areas of the rail, with the use of finite element (FE) modeling. For both 100-8 and 115RE rail, four types of joint bar (defined in the section on joint bar design) with five cross-tie support cases (defined in the section on cross-tie support configuration) were simulated in the parametric study under

typical transit loading. Findings were interpreted to better understand the effects of joint bar length and thickness as well as the number of bolts and consequently to provide guidelines for alternative joint bar designs.

NUMERICAL SIMULATION SETUP

FE analysis is one of the most popular and powerful numerical simulation methods for solving complicated structural and mechanical problems. Commercially available Abaqus/CAE software was selected to perform the simulations. Figure 2 is an example of the numerical models in this parametric study, which consists of four major components: 115RE rail, standard joint bar, simplified bolt, and rail extension. The first three components were modeled as

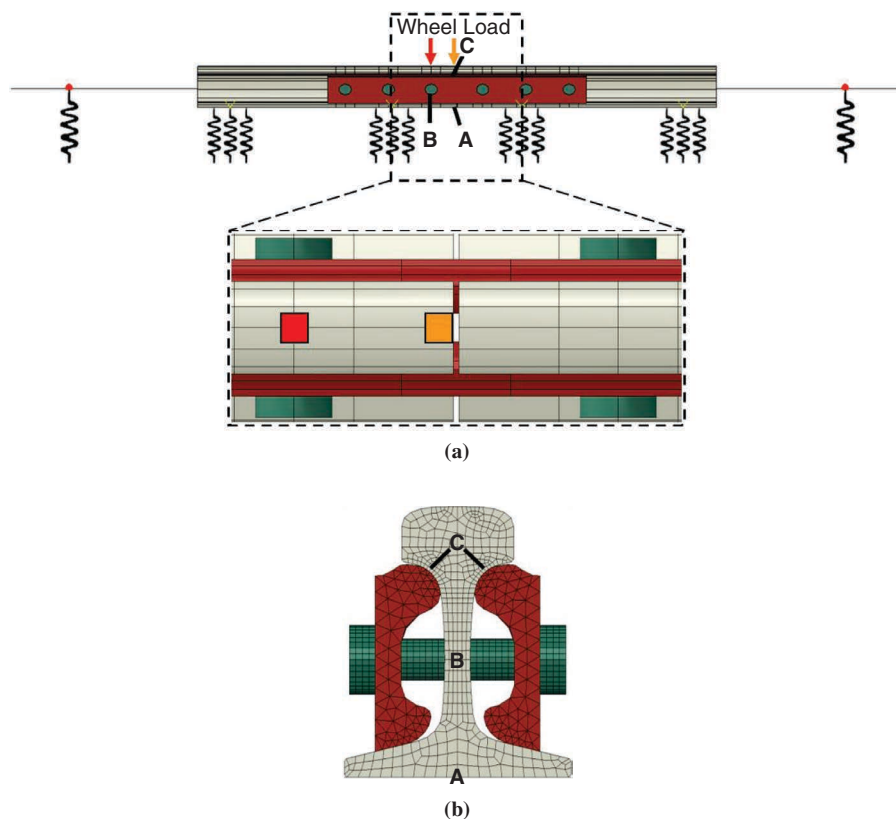


FIGURE 2 FE model of 115RE rail joint: (a) profile and plan views and (b) cross section (A = rail end to capture vertical displacement; B = rail-end bolt hole around which to capture highest tensile and Von Mises stresses; C = rail-end upper fillet to capture the greatest Von Mises stress).

three-dimensional (3-D) deformable solids and the rail extension as deformable wire.

More specifically, the 115RE rail component was meshed with 45,965 linear hexahedron elements, the standard joint bar component with 33,239 linear tetrahedron elements, the simplified bolt component with 2,576 linear hexahedron elements, and the rail extension component with 40 cubic beam elements. The rail extension was assigned the section properties of 115RE rail (i.e., rail cross-sectional area, moment of inertia, and location of the neutral axis). The coefficient of friction between all the components was set at 0.4 (16). The number of elements used may vary when simulating the 100-8 rail and other joint bar designs.

Relevant Simplifications

Like in a previous study, three simplifications were made to the bolted joint models to reduce computational cost for the parametric study (15). First, each rail modeled with 3-D deformable solid elements was only 36 in. (91.4 cm) long, and the remaining 180 in. (457.2 cm) of each rail was simplified by assigning rail section properties to beam elements. Second, the bolt, nut, and washer combination was simplified to a single component with a bolt preload of 22,000 lb (97.9 kN), and the bolt was assumed to be installed perfectly along the central

axis of the rail bolt hole such that initially, no direct contact was captured between bolt shank and rail bolt hole (15). Third, the models were loaded only in the vertical direction so the crossies could be represented by vertical springs. Details of the simplifications are available in an earlier publication (15).

Even though all assumptions and simplifications affect the magnitudes of deflections and stresses calculated with FE modeling, the goal of this study was to compare different configurations. Laboratory experiments are under way, and results will be published in the future.

Variables for Parametric Study

Two rail types, four joint bar designs, five crossie support configurations, and two wheel-loading locations were included in the parametric study. The variables are described in detail in the following subsections.

Rails

Two types of rail section are considered in this parametric study: 100-8 and 115RE, which are representative of rail typically used in heavy rail transit systems. The primary differences between standard joint designs for the two rails are illustrated in Figure 3: the contacting

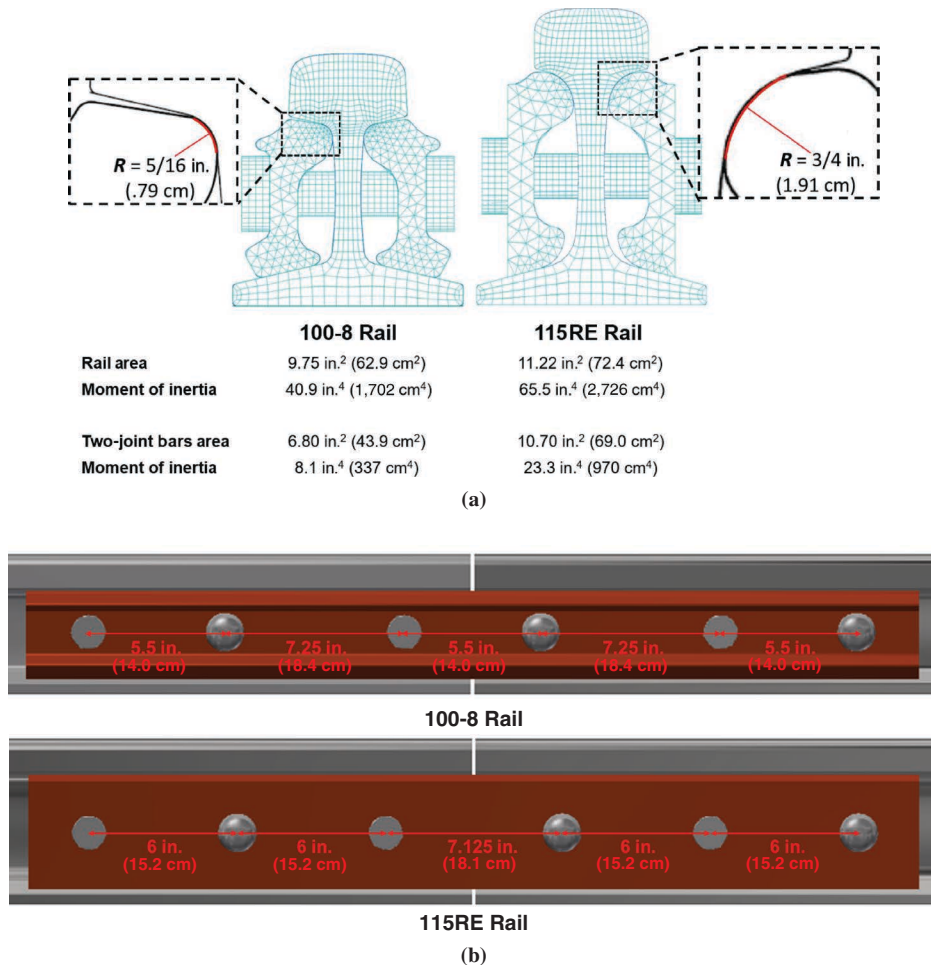


FIGURE 3 Primary differences between standard joint bar for 100-8 rail and 115RE rail: (a) cross section view and (b) profile view.

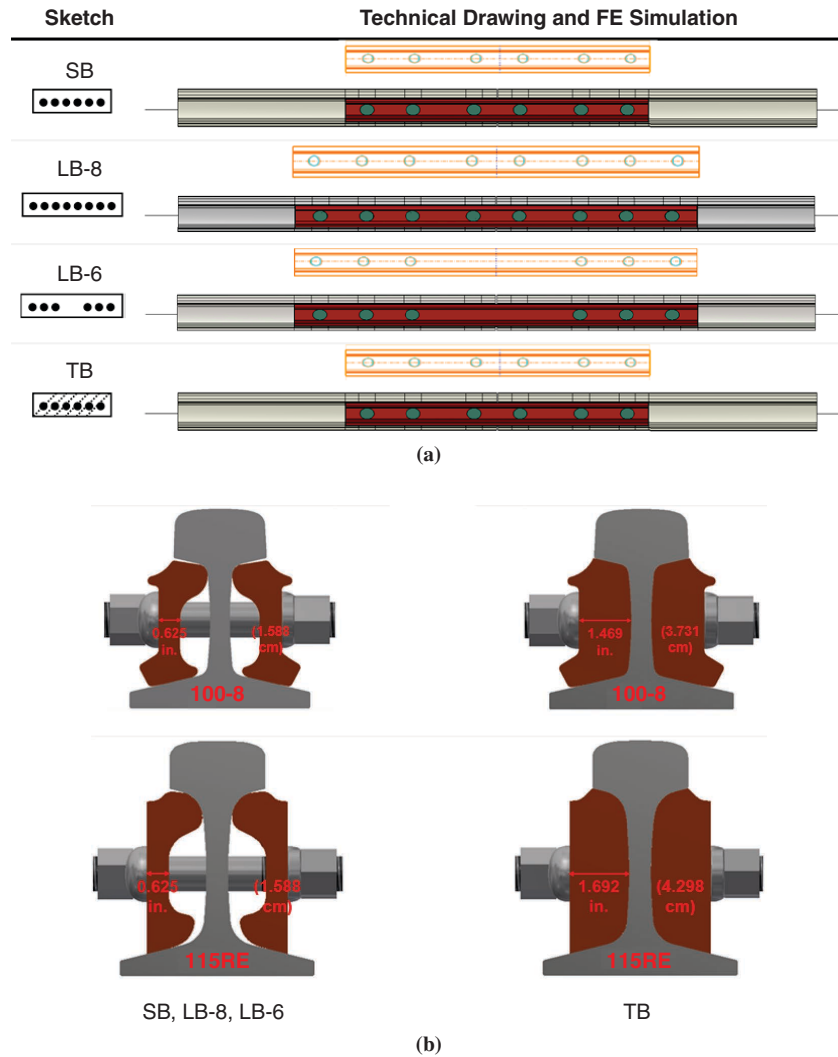


FIGURE 4 Four types of joint bars studied: (a) profile views and (b) cross sections.

area between the rail-end upper fillet and joint bar top of 100-8 rail is considerably smaller than that of 115RE rail, and the cross-sectional area and moment of inertia of 100-8 rail joint bars are noticeably smaller than those of 115RE rail joint bars (Figure 3, *a* and *b*); the locations of the inner four bolt holes also differ (Figure 3, *c* and *d*).

Joint Bar Design

Four types of joint bar are simulated for each rail section in the parametric study: standard joint bar [SB; 36 in. (91.4 cm)], longer bar

with eight holes [LB-8; 48 in. (121.9 cm)], longer bar with six holes [LB-6; 48 in. (121.9 cm)], and thicker bar [TB; 36 in. (91.4 cm)]. Cross sections of the joint bar designs show that for LB-6, rail-end bolt holes are drilled but hidden behind the 48-in. (121.9-cm) joint bar and the inner two bolt holes of the joint bar are undrilled (Figure 4).

Table 1 shows three of the most critical joint bar design properties: thickness at bolt hole, joint bar cross-sectional area, and moment of inertia. The bolt hole is 135% thicker for the TB than for the SB or the LBs for 100-8 rail [1.469 in. (3.7 cm) versus 0.625 in. (1.6 cm), respectively] and 171% thicker for 115RE rail [1.692 in. (4.3 cm) versus 0.625 in. (1.6 cm), respectively]. For 100-8 rail, the cross-

TABLE 1 Critical Properties of Joint Bars for 100-8 and 115RE Rail

| | 100-8 Rail | | 115RE Rail | |
|-------------------------------------|--|--|---|---|
| | SB, LB-8, LB-6 | TB | SB, LB-8, LB-6 | TB |
| Thickness at bolt hole | 0.625 in. (1.6 cm) | 1.469 in. (3.7 cm) | 0.625 in. (1.6 cm) | 1.692 in. (4.3 cm) |
| Two joint bars cross sectional area | 6.80 in. ² (43.9 cm ²) | 10.16 in. ² (65.5 cm ²) | 10.70 in. ² (43.9 cm ²) | 13.84 in. ² (89.3 cm ²) |
| Moment of inertia | 8.10 in. ⁴ (337.1 cm ⁴) | 9.75 in. ⁴ (405.8 cm ⁴) | 23.30 in. ⁴ (969.8 cm ⁴) | 26.51 in. ⁴ (1,103.4 cm ⁴) |

sectional area of the two joint bars is 49.4% greater [10.16 in.² (65.5 cm²) versus 6.80 in.² (43.9 cm²), respectively] for the TB than the SB or LBs, and the moment of inertia is 20.4% greater [9.75 in.⁴ (405.8 cm⁴) versus 8.10 in.⁴ (337.1 cm⁴), respectively]. For 115RE rail, the cross-sectional area of the two joint bars is 29.3% greater for the TB than the SB or LBs [13.84 in.² (89.3 cm²) versus 10.70 in.² (43.9 cm²), respectively], and the moment of inertia is 13.7% greater [26.51 in.⁴ (1,103.4 cm⁴) versus 23.30 in.⁴ (969.8 cm⁴), respectively].

Crosstie Support Configuration

Varying the support condition is a key area of study for this research. The five crosstie support configurations used in the parametric study are described here and illustrated in Figure 5:

- Case A. Nominal [rail joint is suspended in the middle of two crossties spaced 18 in. (45.72 cm) apart];
- Case B. Suspended [rail joint is suspended in the middle of two crossties spaced 22.5 in. (57.15 cm) apart];
- Case C. Supported (crosstie) [rail joint is supported by a crosstie immediately under the center of the joint];
- Case D. Supported (plate edge) [rail joint is supported by the edge of a plate, and center of the crosstie is 3.5 in. (8.89 cm) from the center of the joint]; and
- Case E. Broken plate [crosstie underneath the joint is 5 in. (12.70 cm) away from the center, with its plate broken or missing].

These five cases represent typical crosstie support configurations in the field or worst-case scenarios that might aggravate the material fatigue.

Track Stiffness and Wheel Loading

The track stiffness value adopted in this parametric study is 4,000 psi (27.6 MPa), obtained from field measurements collected on New York City Transit Authority (NYCTA) infrastructure during prior efforts. In addition, 4,000 psi (27.6 MPa) is close to the typical track stiffness measured in regular ballasted track [3,000 psi (20.7 MPa)]. The static wheel load of 16,500 lb (73.4 kN) per wheel also was obtained from NYCTA and is heavier than wheel loads for other heavy rail transit systems. However, the heaviest static wheel load among freight systems can be much higher at 32,000 to 39,000 lb (142.3 to 173.5 kN) per wheel.

The wheel load impact factor varies by condition (e.g., train speed, track stiffness at the joint, or irregularity in wheel or rail shape), especially at rail joints. For this paper, the impact factor was set as a constant of 3.0 on the basis of the current value in the *Manual for Railway Engineering*, which suggests a 200% increase over static vertical loads to estimate the dynamic effect of wheel and rail irregularities (17).

For the simulations conducted and analyzed in this paper, wheel load was applied at two locations: on top of the rail-end bolt hole and on the rail end (Figure 2a). These locations were selected according

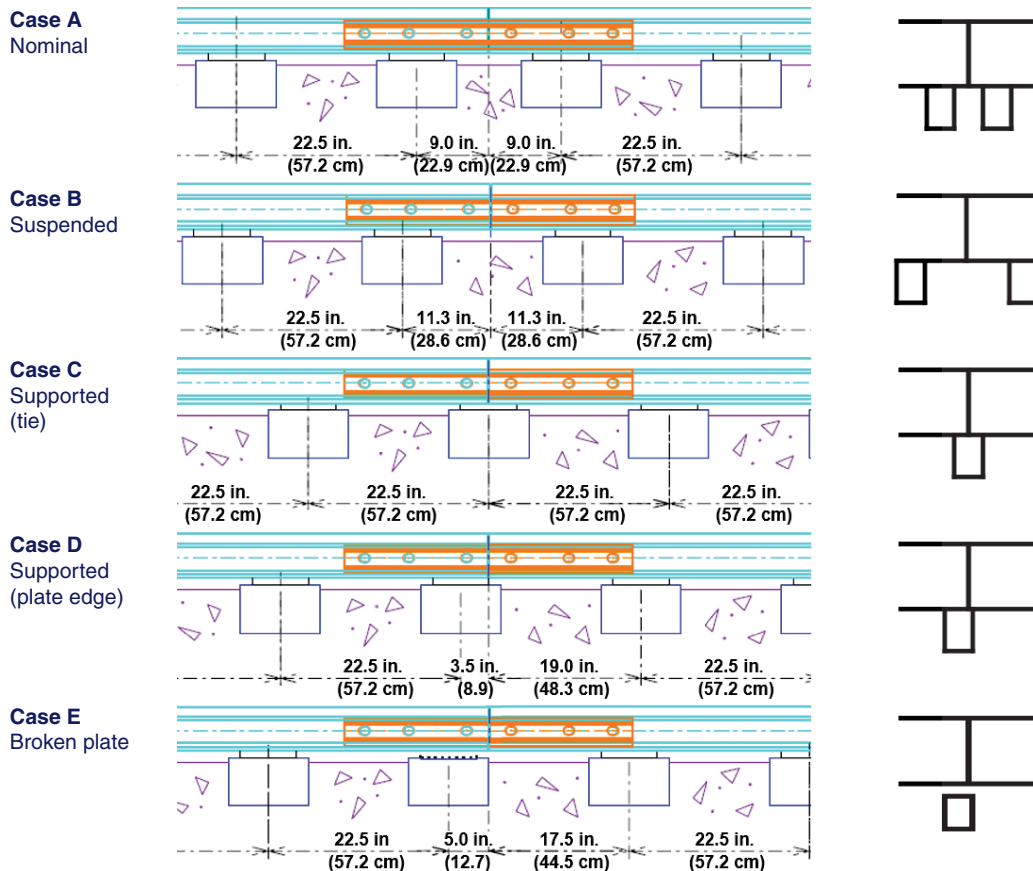


FIGURE 5 The five crosstie support configurations used in the parametric study, each shown in profile and as a simplified sketch.

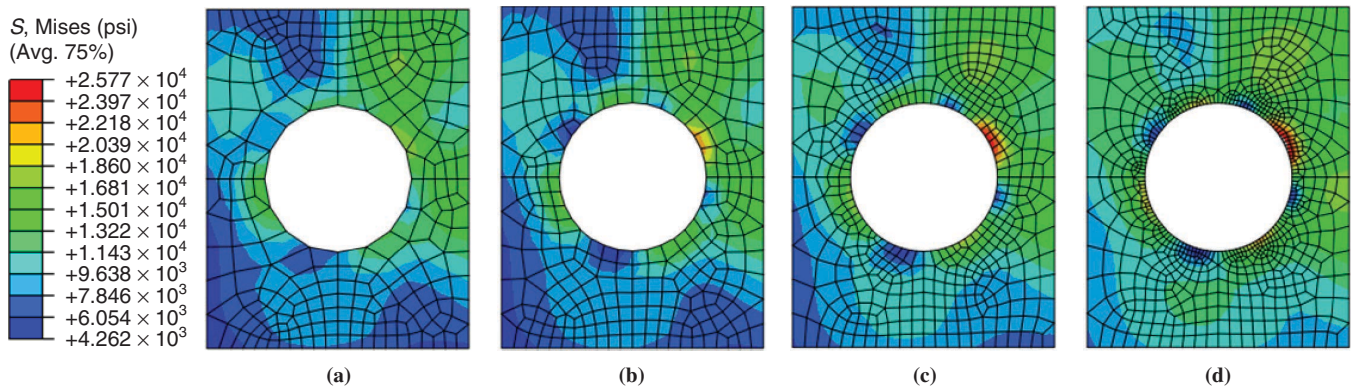


FIGURE 6 Mesh sensitivity analysis around rail-end bolt hole: (a) 16 nodes, (b) 32 nodes, (c) 64 nodes, and (d) 128 nodes (S, Mises = Von Mises stress; 1 psi = 6.89 kPa).

to results of prior FE model simulations conducted at UIUC, which indicated that the rail-end bolt hole stress value reaches its maximum when the wheel is directly above it and that the rail-end upper fillet stress reaches its maximum when the wheel is at the rail end (15).

Model Optimization

Mesh sensitivity analysis was accomplished by comparing the maximum Von Mises stress values around rail-end bolt hole as the number of nodes around that rail-end bolt hole increased. In this sensitivity analysis, four mesh densities were tested by uniformly spreading 16, 32, 64, and 128 nodes around the rail-end bolt hole (Figure 6). The difference between the 64- and 128-node plots is difficult to distinguish, and the maximum Von Mises stress increases from 25,770 to 26,310 psi (177.7 to 181.4 MPa)—only 2.1%. Therefore, to optimize computational accuracy and expense, a mesh density of 64 nodes was selected for the parametric study.

Wire elements were used to simplify the rail at both sides away from the rail section simulated with 3-D solid elements. To avoid a boundary effect and ensure that simulations were accurate and efficient, optimal lengths of 3-D rail section and wire rail extension were determined via a process of trial and error. For this study, the optimal length was 36 in. (91.4 cm) for 3-D rail sections at each side or 72 in. (182.9 cm) total length for the entire 3-D rail in the model, in agreement with the value in the literature (3, 5).

DISCUSSION OF RESULTS

To compare the performance of the four joint bar designs, the three critical outputs of the 100-8 and 115RE rail joint models (vertical displacement at rail end, tensile stress around rail-end bolt hole, and Von Mises stress at rail-end upper fillet) were calculated and plotted with the five crosstie support configurations (Cases A through E). Figure 7 presents an example setup and results for joints with an SB under a wheel load with an impact factor of 3.0 applied on top of the rail-end bolt hole with Case B for 100-8 and 115RE rails.

Vertical Deflection at Rail End

Maximum deflections at rail end are presented in Figure 8 for 100-8 and 115RE rail with four joint bar designs and five crosstie support configurations. The wheel load was applied on top of the rail end

with an impact factor of 3.0, which could lead to larger deflections at the rail end (15). Track modulus was set as 4,000 psi (27.6 MPa), corresponding to the use of resilient plate referenced earlier. Sketches of the five crosstie support configurations appear along the x -axis.

Vertical deflection generally was smaller in 115RE rail than in 100-8 rail, probably because of a higher rail joint stiffness in 115RE rail (Figure 8, Figure 3, Table 1). Differences were greatest between models with a broken plate configuration (Case E), which decrease from around 0.43 in. (1.09 cm) for 100-8 rail to around 0.30 in. (0.76 cm) for 115RE rail.

Overall trends for the effects of different support configurations are similar in 100-8 and 115RE rail sections. Deflections are largest in models with a Case E configuration because joint stiffness decreases drastically with a broken plate. The models with a supported joint configuration (Case C or D) have the smallest deflections because joint stiffness is higher. The models with a suspended joint configuration (Case A or B) have deflections larger than those with Case C or D, and those with Case B configuration exhibit greater deflection than those with Case A configuration because of a longer span.

The longer bar designs LB-8 and LB-6 [48 in. (121.92 cm)] and the standard joint bar SB perform similarly. The LB-6 has more deflection than the SB. However, vertical deflection always is less with the TB than with the SB. In the model with the Case E configuration and the TB, for example, vertical deflection is approximately 12.7% less for 100-8 rail [from 0.43 to 0.37 in. (from 1.09 to 0.95 cm)] and by 6.5% for 115RE rail [from 0.29 to 0.27 in. (from 0.74 to 0.69 cm)].

Tensile Stress Around Rail-End Bolt Hole

Maximum tensile stresses around rail-end bolt hole are presented in Figure 9 for 100-8 and 115RE rail with four joint bar designs and five crosstie support configurations. The wheel load was applied on top of rail-end bolt hole with an impact factor of 3.0, which could lead to larger stresses on the bolt hole (15). The red dashed line shows the material fatigue limit of 61.5 ksi (424.0 MPa), which was estimated as 35% of ultimate tensile strength (18).

The maximum rail-end bolt hole tensile stresses of 115RE rail generally are smaller than those of 100-8 rail, probably because of greater stiffness and smaller deflections at a 115RE rail joint (Figure 9). Results for both 100-8 and 115RE rail are well below the material fatigue limit of 61.5 ksi (424.0 MPa).

Trends for the effects of different support configurations differ for 100-8 rail and 115RE rail. For 100-8 rail, tensile stresses around

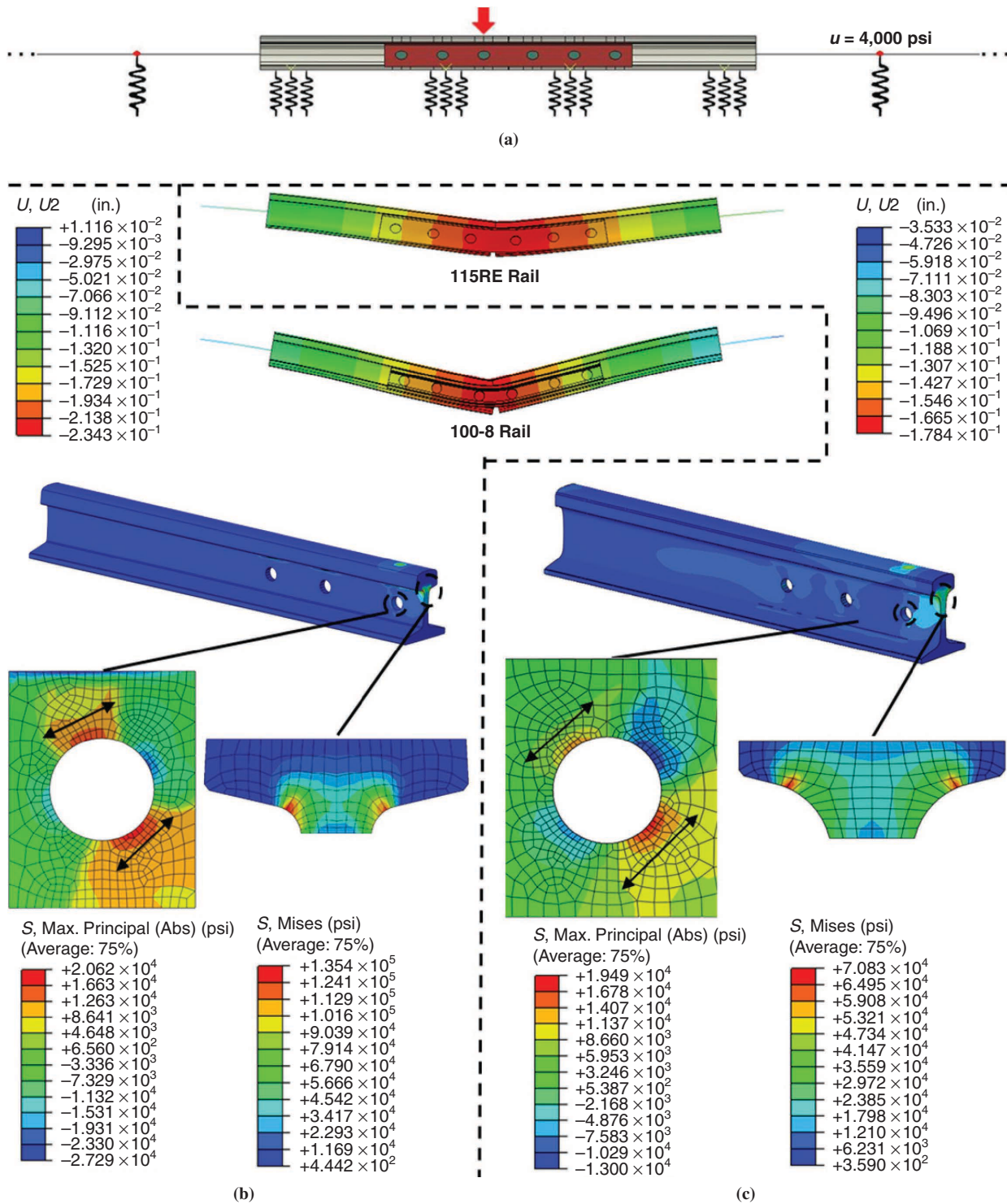


FIGURE 7 Examples for SB joints with Case B crosstie support: (a) loading condition and support configuration, (b) 100-8 rail model results, and (c) 115RE rail model results ($U, U2$ = vertical deflection; $S, \text{ max. principal (abs)}$ = absolute value of maximum principal stress; deformation scale factor = 50; 1 in. = 2.54 cm; 1 psi = 6.89 kPa).

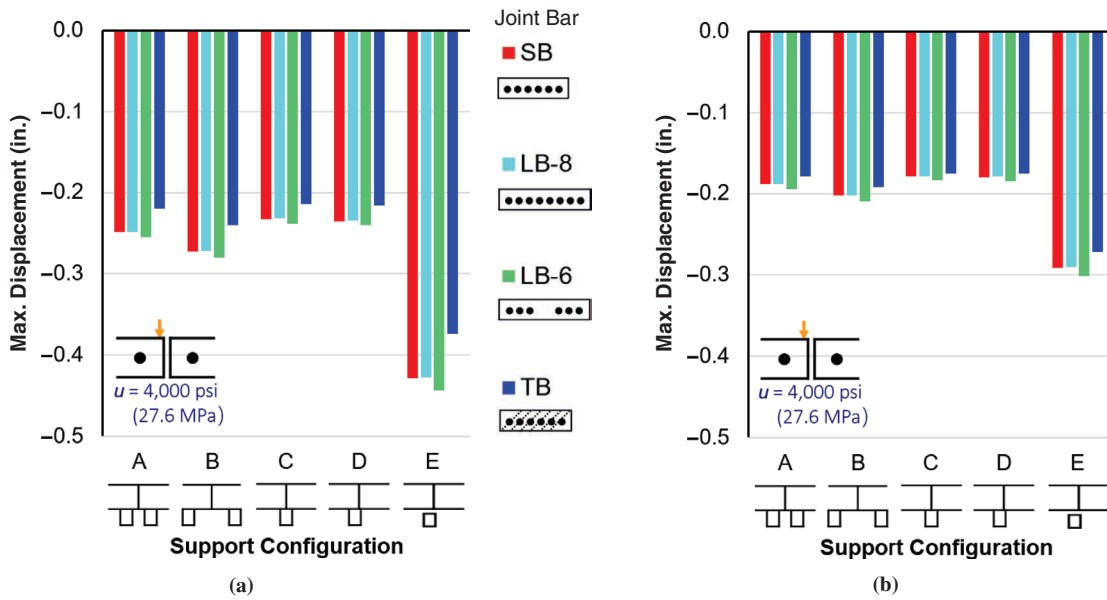


FIGURE 8 Maximum vertical displacement at rail end for four joint bar designs and five support configurations on two rail types: (a) 100-8 and (b) 115RE (u = track modulus; 1 in. = 2.54 cm).

rail-end bolt hole are similar in models with suspended joint configurations (Cases A and B) and in models with supported joint configurations (Cases C and D). For 115RE rail, models with a Case A or B configuration have larger tensile stresses than models with a Case C or D configuration. For both rail types, tensile stresses always are largest in models with a Case E configuration.

Joint bar designs perform differently for 100-8 and 115RE rails. The tensile stress of the LB-8 generally is similar to that of the SB

for 100-8 rail but higher than that of the SB for 115RE rail. The tensile stress of the LB-6 generally was higher than that of the SB for 100-8 rail, except in models with the Case E configuration; however, tensile stress of LB-6 was lower than that of SB for 115RE rail in models with a Case A, B, or E configuration. With all support configurations, tensile stress in the end bolt hole was considerably higher in models with the TB than in models with the SB for 100-8 rail and similar in models with the TB or the SB for 115RE rail.

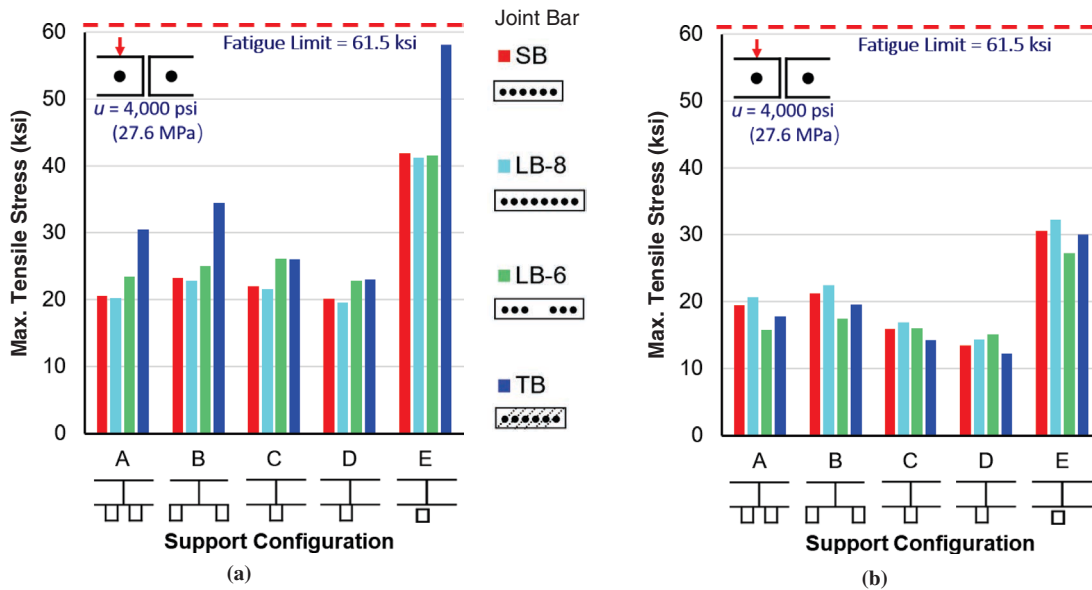


FIGURE 9 Maximum tensile stress around rail-end bolt hole for four joint bar designs and five support configurations on two rail types: (a) 100-8 and (b) 115RE (1 ksi = 6.89 MPa).

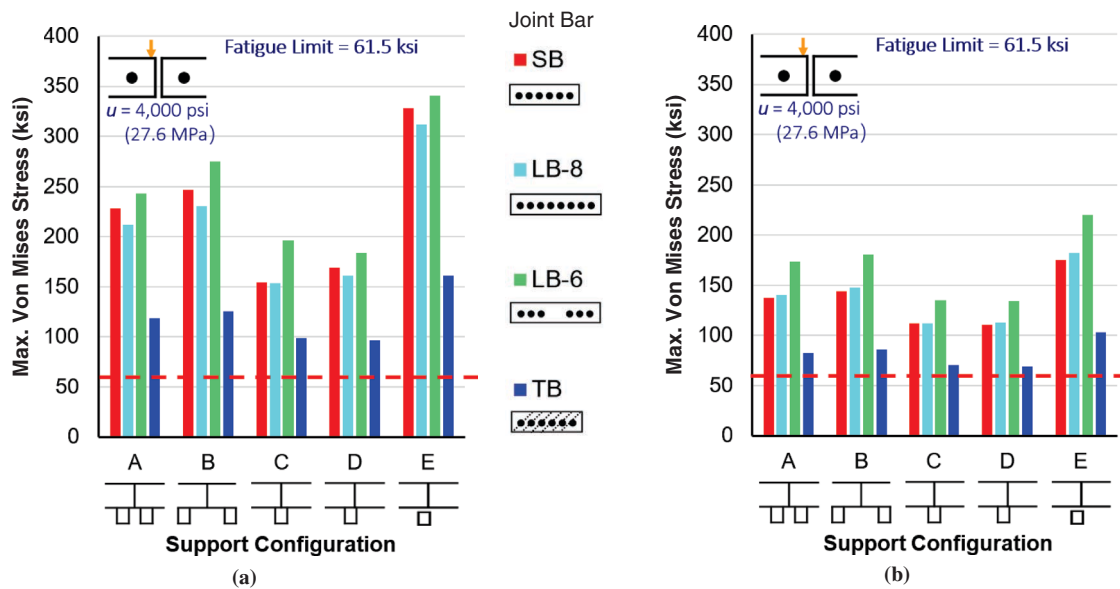


FIGURE 10 Maximum Von Mises stress around rail-end upper fillet for four joint bar designs and five support configurations on two rail types: (a) 100-8 and (b) 115RE.

Von Mises Stress at Rail-End Upper Fillet

The maximum Von Mises stresses at the rail-end upper fillet are presented in Figure 10 for 100-8 and 115RE rail with four joint bar designs and five crosstie support configurations. The wheel load was applied on top of the rail end with an impact factor of 3.0, which could lead to larger stresses in the upper fillet (15). The red dashed line shows the material fatigue limit of 61.5 ksi (424.0 MPa).

Maximum Von Mises stresses in the rail-end upper fillet generally are smaller in 115RE rail than in 100-8 rail, probably because of a greater stiffness and smaller deflections at the 115RE rail joint. More important, the results of both 100-8 and 115RE rail exceed the material fatigue limit of 61.5 ksi (424.0 MPa).

Overall trends for the support configurations are similar for 100-8 and 115RE rail. The models with a suspended joint configuration (Case A or B) have greater Von Mises stresses in the rail-end upper fillet than models with a supported joint configuration (Case C or D). The Von Mises stresses at the rail-end upper fillet always are largest in models with the broken plate configuration (Case E).

In general, Von Mises stresses in the rail-end upper fillet with LB-8 and LB-6 were similar to or higher than those with the SB. However, Von Mises stresses were lower in the rail-end upper fillet with the TB than with the SB. In the model with the broken plate configuration (Case E), for example, adopting the TB can reduce maximum stress in the rail-end upper fillet by approximately 51% for 100-8 rail [from 328.5 to 161.1 ksi (2,265 to 1,111 MPa)] and by 41% for 115RE rail [from 175.3 to 102.9 ksi (1,209 to 710 MPa)].

CONCLUSIONS

The results of detailed numerical simulations of the stress distribution around the rail-end bolt hole and rail-end upper fillet areas are presented for 100-8 and 115RE rail. Four joint bar designs were simulated

and compared: a standard joint bar, a longer joint bar with eight holes, a longer joint bar with six holes, and a thicker joint bar.

The following conclusions can be drawn from the results of this study:

1. For stress distribution in rail-end bolt hole and upper fillet areas, the LB-6 and LB-8 generally performed the same as the SB in the same rail section. In other words, longer joint bars did not noticeably improve performance.
2. Stress in the rail upper fillet with Case E was up to 51% lower in 100-8 rail and 41% lower in 115RE rail with the TB than with the SB. Thus, the TB may be used to reduce or prevent rail fillet cracks.
3. When evaluating joint bar designs, the rail and joint bar must be considered together, as a system, because the performance of one joint bar design might change with different rail sections. For 100-8 rail, the TB can reduce stress in the rail upper fillet but will increase stress in the rail-end bolt hole; for 115RE rail, the TB can reduce stress in the rail upper fillet without increasing stress in the rail-end bolt hole.

ACKNOWLEDGMENTS

This research was funded in part by WSP–Parsons Brinckerhoff, under a contract with the New York City Transit Authority (NYCTA), and the National University Rail Center. Portions of this paper are based on background information that was provided under a broader research program for WSP–Parsons Brinckerhoff and NYCTA. The authors thank WSP–Parsons Brinckerhoff, NYCTA Inspections and Testing, and NYCTA Track Engineering for providing leadership and oversight for the broader work with which this paper is associated. The authors also thank Don Uzarski and Michael Yang of the University of Illinois at Urbana–Champaign (UIUC) and Michael Carolan of Volpe National Transportation Systems Center for assistance and advice. The third author was supported in part

by grants to the UIUC Rail Transportation and Engineering Center (RailTEC) from CN, Hanson Professional Services, and the George Krambles Transportation Scholarship Fund.

REFERENCES

1. Tratman, E. E. R. *Railway Track and Track Work*. The Engineering News Publishing Company, New York, 1897.
2. *Improvement in Railroad Rail-Joints*. US132988 A. U.S. Patent Office, 1872.
3. *Angle-Splice for Railway-Joint*. US228347 A. U.S. Patent Office, 1880.
4. *Railway Joint*. US416150 A. U.S. Patent Office, 1889.
5. Charlton, Z.I. *Innovative Design Concepts for Insulated Joints*. Master's thesis. Virginia Polytechnic Institute and State University, Blacksburg, 2007.
6. Raymond, W.G. *The Elements of Railroad Engineering*, 4th ed. John Wiley & Sons, Inc., New York, 1923.
7. *Derailment and Subsequent Collision of Two Metro-North Passenger Trains*. Railroad Accident Brief NTSB/RAB-14/09. National Transportation Safety Board, Oct. 24, 2014.
8. Schlesinger, D. 2016. Sources of Transportation Accident Information. *Proceedings of the 2016 Joint Rail Conference*, Columbia, S.C., April 2016. 10.1115/JRC2016-5836.
9. Orringer, O., J.M. Morris, and R.K. Steele. Applied Research on Rail Fatigue and Fracture in the United States. *Theoretical and Applied Fracture Mechanics*, Vol. 1, No. 1, 1984, pp. 23–49. [http://dx.doi.org/10.1016/0167-8442\(84\)90019-3](http://dx.doi.org/10.1016/0167-8442(84)90019-3).
10. Jeong, D.Y. *Progress in Rail Integrity Research. Final Report*. DOT/FRA/ORD-01/18. FRA, U.S. Department of Transportation, October 2001.
11. Mayville, R.A., and P.D. Hilton. Fracture Mechanics Analysis of a Rail-End Bolt Hole Crack. *Theoretical and Applied Fracture Mechanics*, Vol. 1, No. 1, 1984, pp. 51–60. [http://dx.doi.org/10.1016/0167-8442\(84\)90020-X](http://dx.doi.org/10.1016/0167-8442(84)90020-X).
12. Mayville, R.A., and R.G. Stringfellow. *Development and Application of Rail Defect Fracture Models to Assess Remedial Actions. Final Report*. DOT/FRA/ORD-93/33. FRA, U.S. Department of Transportation, August 1993.
13. Mayville, R.A., and R.G. Stringfellow. Numerical Analysis of a Railroad Bolt Hole Fracture Problem. *Theoretical and Applied Fracture Mechanics*, Vol. 24, No. 1, 1995, pp. 1–12. [http://dx.doi.org/10.1016/0167-8442\(95\)00026-B](http://dx.doi.org/10.1016/0167-8442(95)00026-B).
14. Carolan, M.E., D.Y. Jeong, and A.B. Perlman. Engineering Studies on Joint Bar Integrity, Part II: Finite Element Analysis. *Proceedings of the 2014 Joint Rail Conference*, April 2014, Colorado Springs, Colo., 2014.
15. Zhu, K., J.R. Edwards, Y. Qian, and B. Andrawes. Finite Element Analysis of the Effects of Bolt Condition on Bolted Rail Joints Stresses. *Transportation Research Record: Journal of the Transportation Research Board*, No. 2545, 2016, pp. 36–45. <http://dx.doi.org/10.3141/2545-05>.
16. Wen, Z., X. Jin, and W. Zhang. Contact-Impact Stress Analysis of Rail Joint Region Using the Dynamic Finite Element Method. *Wear*, Vol. 258, No. 7, 2005, pp. 1301–1309. <http://dx.doi.org/10.1016/j.wear.2004.03.040>.
17. American Railway Engineering and Maintenance-of-Way Association. *Manual for Railway Engineering, Volume 1: Track*, Chapter 4: Rail. Lanham, Md., 2016.
18. Zhu, K., J.R. Edwards, Y. Qian, and B. Andrawes. Fatigue Analysis of Rail-Head-to-Web Fillet at Bolted Rail Joint Under Various Impact Wheel Load Factors and Support Configurations. *Proceedings of the 2016 Joint Rail Conference*, Columbia, S.C., April 2016. 10.1115/JRC2016-5802.

The opinions expressed in this paper are those of the authors and do not represent the opinions of the funding agency.

The Standing Committee on Railway Maintenance peer-reviewed this paper.